Assessing light scattering of intracellular organelles in single intact living cells

Maxim Kalashnikov[1], Wonshik Choi[1,2*], Chung-Chieh Yu[1], Yongjin Sung[1], Ramachandra R. Dasari[1], Kamran Badizadegan[1,3], and Michael S. Feld[1]

[1]*G. R. Harrison Spectroscopy Laboratory, Massachusetts Institute of Technology, Cambridge, Massachusetts 02139, USA*

[2]*Department of Physics, Korea University, Seoul 136-701, Korea*

[3]*Department of Pathology, Harvard Medical School and Massachusetts General Hospital, Massachusetts 02114, USA*

**wonshik@mit.edu.*

Abstract: This report presents a model-independent method of assessing contributions to the light scattering from individual organelles in single intact cells. We first measure the 3D index map of a living cell, and then modify the map in such a way so as to eliminate contrast due to a particular intracellular organelle. By calculating and comparing the light scattering distributions calculated from the original and modified index maps using the Rytov approximation, we extract the light scattering contribution from the particular organelle of interest. The relative contributions of the nucleus and nucleolus to the scattering of the entire cell are thus determined, and the applicability of the homogeneous spherical model to non-spherical and heterogeneous organelles in forward scattering is evaluated.

OCIS codes: (170.1530) Cell analysis; (290.2558) Forward scattering; (290.4020) Mie theory; (290.5820) Scattering measurements; (170.6510) Spectroscopy, tissue diagnostics.

References and links

1. V. Backman, R. Gurjar, K. Badizadegan, L. Itzkan, R. R. Dasari, L. T. Perelman, and M. S. Feld, "Polarized light scattering spectroscopy for quantitative measurement of epithelial cellular structures in situ," IEEE J. Sel. Top. Quantum Electron. **5**(4), 1019–1026 (1999).
2. C. Mujat, C. Greiner, A. Baldwin, J. M. Levitt, F. Tian, L. A. Stucenski, M. Hunter, Y. L. Kim, V. Backman, M. Feld, K. Münger, and I. Georgakoudi, "Endogenous optical biomarkers of normal and human papillomavirus immortalized epithelial cells," Int. J. Cancer **122**(2), 363–371 (2008).
3. H. Fang, M. Ollero, E. Vitkin, L. M. Kimerer, P. B. Cipolloni, M. M. Zaman, S. D. Freedman, I. J. Bigio, I. Itzkan, E. B. Hanlon, and L. T. Perelman, "Noninvasive sizing of subcellular organelles with light scattering spectroscopy," IEEE J. Sel. Top. Quantum Electron. **9**(2), 267–276 (2003).
4. R. S. Gurjar, V. Backman, L. T. Perelman, I. Georgakoudi, K. Badizadegan, I. Itzkan, R. R. Dasari, and M. S. Feld, "Imaging human epithelial properties with polarized light-scattering spectroscopy," Nat. Med. **7**(11), 1245–1248 (2001).
5. M. Hunter, V. Backman, G. Popescu, M. Kalashnikov, C. W. Boone, A. Wax, V. Gopal, K. Badizadegan, G. D. Stoner, and M. S. Feld, "Tissue self-affinity and polarized light scattering in the born approximation: A new model for precancer detection," Phys. Rev. Lett. **97**(13), 138102 (2006).
6. J. R. Mourant, T. M. Johnson, S. Carpenter, A. Guerra, T. Aida, and J. P. Freyer, "Polarized angular dependent spectroscopy of epithelial cells and epithelial cell nuclei to determine the size scale of scattering structures," J. Biomed. Opt. **7**(3), 378–387 (2002).
7. A. Wax, C. Yang, V. Backman, K. Badizadegan, C. W. Boone, R. R. Dasari, and M. S. Feld, "Cellular Organization and Substructure Measured Using Angle-Resolved Low-Coherence Interferometry," Biophys. J. **82**(4), 2256–2264 (2002).
8. A. Wax, C. Yang, M. G. Müller, R. Nines, C. W. Boone, V. E. Steele, G. D. Stoner, R. R. Dasari, and M. S. Feld, "In Situ Detection of Neoplastic Transformation and Chemopreventive Effects in Rat Esophagus Epithelium Using Angle-resolved Low-coherence Interferometry," Cancer Res. **63**(13), 3556–3559 (2003).
9. J. D. Wilson, and T. H. Foster, "Mie theory interpretations of light scattering from intact cells," Opt. Lett. **30**(18), 2442–2444 (2005).
10. M. Xu, T. T. Wu, and J. A. Y. Qu, "Unified Mie and fractal scattering by cells and experimental study on application in optical characterization of cellular and subcellular structures," J. Biomed. Opt. **13**, (2008).

#115619 - $15.00 USD Received 13 Aug 2009; revised 27 Sep 2009; accepted 28 Sep 2009; published 15 Oct 2009

11. C. C. Yu, C. Lau, J. W. Tunnell, M. Hunter, M. Kalashnikov, C. Fang-Yen, S. F. Fulghum, K. Badizadegan, R. R. Dasari, and M. S. Feld, "Assessing epithelial cell nuclear morphology by using azimuthal light scattering spectroscopy," Opt. Lett. **31**(21), 3119–3121 (2006).
12. A. Brunsting, and P. F. Mullaney, "Differential Light Scattering from Spherical Mammalian Cells," Biophys. J. **14**(6), 439–453 (1974).
13. R. M. P. Doornbos, M. Schaeffer, A. G. Hoekstra, P. M. A. Sloot, B. G. deGrooth, and J. Greve, "Elastic light-scattering measurements of single biological cells in an optical trap," Appl. Opt. **35**(4), 729–734 (1996).
14. V. P. Maltsev, "Scanning flow cytometry for individual particle analysis," Rev. Sci. Instrum. **71**(1), 243–255 (2000).
15. V. P. Maltsev, and K. A. Semyanov, *Characterisation of Bio-Particles from Light Scattering* (VSP, Utrecht, 2004).
16. A. E. Zharinov, P. A. Tarasov, A. N. Shvalov, K. A. Semyanov, D. R. van Bockstaele, and V. P. Maltsev, "A study of light scattering of mononuclear blood cells with scanning flow cytometry," J. Quant. Spectrosc. Radiat. Transf. **102**(1), 121–128 (2006).
17. W. Choi, C. Fang-Yen, K. Badizadegan, S. Oh, N. Lue, R. R. Dasari, and M. S. Feld, "Tomographic phase microscopy," Nat. Methods **4**(9), 717–719 (2007).
18. W. Choi, C. C. Yu, C. Fang-Yen, K. Badizadegan, R. R. Dasari, and M. S. Feld, "Field-based angle-resolved light-scattering study of single live cells," Opt. Lett. **33**(14), 1596–1598 (2008).
19. Y. Sung, W. Choi, C. Fang-Yen, K. Badizadegan, R. R. Dasari, and M. S. Feld, "Optical diffraction tomography for high resolution live cell imaging," Opt. Express **17**(1), 266–277 (2009).
20. A. J. Devaney, "Inverse-scattering theory within the Rytov approximation," Opt. Lett. **6**(8), 374–376 (1981).
21. E. Wolf, "Three-dimensional structure determination of semi-transparent objects from holographic data," Opt. Commun. **1**(4), 153–156 (1969).
22. H. Hulst, *Light scattering by small particles* (Dover Publications, New York, 1981).
23. C. L. Curl, C. J. Bellair, T. Harris, B. E. Allman, P. J. Harris, A. G. Stewart, A. Roberts, K. A. Nugent, and L. M. D. Delbridge, "Refractive index measurement in viable cells using quantitative phase-amplitude microscopy and confocal microscopy," Cytometry A **65A**(1), 88–92 (2005).
24. K. F. A. Ross, *Phase contrast and interference microscopy for cell biologists* (Edward Arnold Ltd, London, 1967).
25. R. Barer, K. F. A. Ross, and S. Tkaczyk, "Refractometry of living cells," Nature **171**(4356), 720–724 (1953).

1. Introduction

Light scattering spectroscopy has emerged as a valuable tool for cancer diagnosis over the past ten years. Morphological information, critical to disease diagnoses, has been extracted from both angle and wavelength-dependent light scattering distributions based on simplified cell models. Light scattered from the cellular structures provides information about the morphological changes accompanying early stage malignancy. The virtue of this technique lies in the ability to extract key morphological information such as size distributions of nucleus and submicron-sized particles with minimal data acquisition, mainly due to model-based data analysis [1–11]. These studies have focused on the basic morphology and biochemistry of normal and cancerous cells [1–3, 6, 7, 9, 10, 12], animal models of cancer development [5, 8] and human tissue studies in laboratory and clinical settings [1, 4, 11]. The validity of the extracted information, however, tends to be highly dependent on the accuracy of the cell/tissue scattering models, which typically pose constraints on the specimen under study. Hence, the sensitivity of the method for different models can hamper its usefulness for basic cell research and its clinical applications.

Light scattering is governed by the 3D distribution of the object's complex refractive index, i.e. its absorption coefficient and refractive index. Typical light scattering measurements take place in the angular plane, and either the angular distribution at a given wavelength or the spectral distribution at a fixed angle are utilized to extract morphological information of a specimen. Considering that the specimen is a 3D object and that measurements are typically performed in only 1D or 2D, the inverse problem is highly underdetermined. In order to determine the 3D complex refractive index distribution of an object, and hence its morphology, the complex E-field of scattered light must be measured at various illumination angles or at multiple wavelengths. However, when the scattering object is assumed to be spherical, the required amount of data to solve the inverse problem is greatly reduced. By fitting the light scattering distribution to Mie theory, which assumes spherical scatterers, the size of the object and its mean index contrast can be accurately determined. For

#115619 - $15.00 USD Received 13 Aug 2009; revised 27 Sep 2009; accepted 28 Sep 2009; published 15 Oct 2009

example, in models designed to correlate light scattering with pre-cancer progression in cells, cell nuclei were assumed to be the dominant spherical scatters inside the cell with refractive index contrast n_nuclei/n_cytoplasm = 1.03-1.07 [1, 4, 8, 11], from which the size distribution could be extracted from the light scattering distribution. However, the shapes of the organelles are far from spherical and their index distributions are heterogeneous. Thus, it would be highly informative to validate if the homogeneous spherical organelle model is a good approximation to more realistic organelles.

The conventional light scattering instruments have two major limitations in rigorous validation of cell models. First, most of the instruments have insufficient sensitivity to detect individual cells. Thus, light scattering from thousands of cells needs to be accumulated and statistical averaging is inevitable. Second, even when the scattering distributions of a single cell were measured, as demonstrated by some of the advanced light scattering instruments [13–15] which could eliminate the effect of statistical averaging, only the outermost dimension and an average index of the whole cell were characterized in most cases. The low dimensionality of the data (1D or 2D) requires extensive parametric modeling to solve the inverse scattering problem for the inner structure of the cell in either single cell experiments [16] or multi-cellular data analysis [1–11]. Attempts have been made to isolate the scattering from the various cellular organelles by cell lysing and physical extraction of organelle suspensions [3,6]. However, the equivalence of the structure of the organelles in suspension and in intact cells has not been shown, since the removal process is irreversible.

For a correct interpretation of the scattering, it is crucial to measure the 3D distribution of refractive index in single intact cells. In the recent studies, we implemented tomographic phase microscopy to obtain 3D refractive index distributions in single living cells from E-field measurements at multiple angles of illumination [17], and exploited the connection between the refractive index map and the light scattering distribution of a whole cell based on the Born approximation [18]. In this paper, we extend the previous method in order to determine the light scattering contribution of individual organelles such as the cell nucleus and nucleolus by means of the Rytov approximation, which is more accurate than the Born approximation [19]. From the measured scattering of intracellular organelles, the validity of the model-based approaches is studied and the accuracy of light scattering spectroscopy is explored.

2. Tomographic phase microscopy: E-field based measurements

Using tomographic phase microscopy, we measured the refractive index tomogram of HT29 cells and human colonic adenocarcinoma cells [19]. A He-Ne laser with wavelength of 633 nm was used as an illumination source. Six hundred E-field images were recorded in less than 10 seconds at angles of illumination ranging from −65 to 65 degrees with respect to the optic axis. Optical diffraction tomography based on the Rytov approximation was applied with a constraint algorithm to solve the inverse problem. The lateral slice image of the reconstructed 3D index map, referred to as the tomogram, is presented in Fig. 1(a). Three major sub-cellular organelles can be identified: the cytoplasm (1), the nucleolus (2), and nucleus excluding the nucleolus (3). The Rytov approximation is valid enough in imaging biological cells, and the detailed explanation on the approximation and its experimental validation were covered at length in our previous publication [19]. The accuracy of index measurement was as good as 0.001, and the pixel to pixel variation, or sensitivity of the measurement, was about 0.005.

Next, we implemented an algorithm to calculate angular light scattering, $\left|\hat{U}^{(S)}(k_x,k_y)\right|^2$, for a given 3D distribution of refractive index, n(X, Y, Z), of an arbitrary object. We ignored the absorption coefficient, since absorption of the cell at visible wavelengths is negligible. The Rytov approximation was used along with the Fourier diffraction theorem [20,21], which states that the Fourier transform of the refractive index map has a linear relationship with the Fourier transform of the scattered field as follows.

#115619 - $15.00 USD Received 13 Aug 2009; revised 27 Sep 2009; accepted 28 Sep 2009; published 15 Oct 2009

$$\hat{F}(K_x, K_y, K_z) = \frac{ik_z}{\pi}\hat{U}^{(S)}(k_x, k_y) \quad (1)$$

Here, $F(X,Y,Z) \equiv -(2\pi n_m/\lambda_0)^2((n(X,Y,Z)/n_m)^2 - 1)$ and $U^{(S)} = U^{(I)}(x,y)\ln\frac{U(x,y)}{U^{(I)}(x,y)}$.

The ^ denotes Fourier transform, λ_0 the wavelength of the source in free space, n_m the index of medium, U(x,y) the measured complex E-field at a given illumination E-field of $U^{(I)}$(x, y), respectively. (X,Y,Z) and (x,y,z) are the spatial coordinates in the specimen frame and in the laboratory frame, respectively. (K_x, K_y, K_z) and (k_x, k_y, k_z) are the conjugate spatial frequency coordinates to (X, Y, Z) and (x, y, z), respectively.

Since the wavelength of the source is conserved after the scattering, the spatial frequencies (k_x, k_y) in 2-D scattering intensity distribution of $\left|\hat{U}^{(S)}(k_x, k_y)\right|^2$ can be expressed as polar angle θ and azimuthal angle φ via following equations: $\sqrt{k_x^2 + k_y^2} = n\sin(\theta)/\lambda$ and $\varphi = arctan(k_y/k_x)$, respectively. Thus, the angular light scattering intensity I(θ, φ) is calculated as a square of the scattered field $|U(k_x,k_y)|^2$ after the coordinate conversion. Figure 1(d) shows the angular scattering intensity distribution calculated from the original refractive index map, n(X, Y, Z), when the illumination direction is parallel to the optic axis.

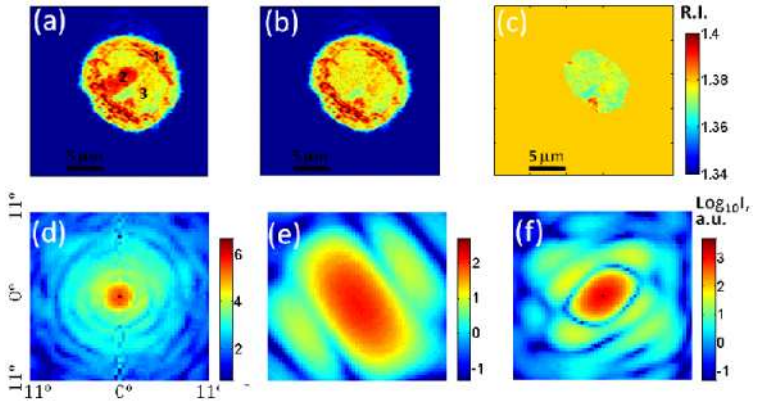

Fig. 1. Cross-section of 3D refractive index tomograms and 2D angular scattering maps: (a) Original tomogram section of HT29 cell and (b) Tomogram section with nucleolus replaced with random nuclear index values. (c) Tomogram of the cell nucleus. The color bar indicates refractive index at wavelength of 633 nm. Scale bars indicate 5 μm. (d) Angular scattering intensity of the original cell tomogram. (e) Scattering intensity of the nucleolus. (f) Angular scattering of the nucleus. The color bar indicates intensity in logarithm base 10 with arbitrary units.

3. Extraction of scattering distribution from individual organelles

In order to assess the contribution to the light scattering from individual organelles, we modified the originally measured 3D index distribution in such a way as to eliminate the contribution of a specific organelle of interest, and calculate the scattering from the modified 3D map. By subtracting the scattering map of the modified tomogram from that of the original tomogram, the contribution of the specific organelle can be determined. Note that this approach is valid within the Rytov approximation in which the change in incident field is assumed to be sufficiently small. We first extracted the scattering distribution of the nucleolus. The region associated with nucleolus (2) was replaced with refractive index values of the rest of the nucleus, drawn according to uniform distribution on a pixel-by-pixel basis (Fig. 1(b)). This procedure was repeated at every section of different heights in which the nucleolus border could be clearly determined, leading to generation of a new 3D tomogram in

#115619 - $15.00 USD Received 13 Aug 2009; revised 27 Sep 2009; accepted 28 Sep 2009; published 15 Oct 2009

which the nucleolus is absent. The difference between scattering fields calculated from the original tomogram and the nucleolus-free tomogram using Eq. (1) thus provides the scattering distribution contributed solely by the nucleolus. Figure 1(e) shows the scattering distribution of nucleolus when the incident beam is parallel to the optic axis. Oscillations in angular distribution are much coarser than those of the whole cell, and the asymmetry of the light scattering distribution was as expected from the asymmetry of the shape. This is the first time to our knowledge that the light scattering of a single nucleolus in an intact living cell has been assessed.

A similar procedure was applied to assess the scattering of the nucleus. In the nucleolus-free tomogram (Fig. 1(b)), there are three major compartments causing light scattering: cell boundary, particles in the cytoplasm and the nucleus. We eliminated the cell boundary and particles in the cytoplasm at every section by setting the index of the surrounding area of nucleus as the average index of cytoplasm (Fig. 1(c)). This modified tomogram contains only the scattering contribution of the nucleus. Using the Rytov approximation described in Eq. (1), nuclear scattering was directly calculated from this modified tomogram (Fig. 1(f)). The oscillations in angular distribution are finer than those of the nucleolus, as expected. As an alternative method, we modified the nuclear region by replacing the index by that of the cytoplasm, and took the difference of the scatterings between the two tomograms. The calculated nuclear scattering was almost the same as with the previous method.

4. Applicability of the spherical scatterer model for intracellular organelles of arbitrary shapes

As mentioned in the introduction, the spherical model of the nucleus has been used in interpreting cell scattering in studying pre-cancer diagnosis. The cell nucleus, however, is generally not spherical, and the internal index distribution is heterogeneous. We assessed the applicability of the spherical model for cell nucleus using refractive index tomograms of live cells. We took the same cell used in Fig. 1 for this analysis in which the nucleus is asymmetric and asymptotically elliptical with the ratio of the major-to-minor axes of 1.37 as shown in Fig. 2(a). In conjunction with the structure, the calculated scattering of the nucleus exhibits asymmetry (Fig. 1(f)). The angular scattering spectra are extracted along the major and minor axes of the nuclear section (solid black lines in Figs. 2(b)-(c)).

Light scattering of a spherical particle can be analyzed by Mie theory, which provides an exact numerical solution to the scattering problem [22]. According to Mie theory, the scattering distribution is determined by the diameter of spherical particle and the relative refractive index contrast between the particle and the surrounding medium. Previously, the relative index m, which is the index ratio between the particle of interest and the medium, was not directly measured. Consequently, in studying scattering of biological tissue samples, both m and the size distribution of the particle were extracted from the data fitting to the theory [1–11]. In our study, the indices of the particle and the medium could be directly measured. This new feature allows us to extract the size distribution of the particle more precisely. We took the average refractive indices of the nucleus (n=1.374) and cytoplasm (n=1.380) from the original index tomogram of the cell. For this given index contrast, we fitted the angular scattering spectra taken along major and minor axes with Mie theory by varying the particle diameter in the range between 1 and 19 μm. Best fits could be attained when the diameters were 7.79 and 9.97 μm, respectively, whereas the corresponding lengths measured from the tomogram were 7.11 and 9.48 μm (Figs. 2(b)-(c)). Therefore, the length of each individual axis in the nuclear tomogram's cross-section could be determined using Mie theory within 10% accuracy or better. The discrepancies between the calculated angular scattering spectra and Mie theory fit were largely due to the effect of heterogeneity of the inner structure in the nucleus. When the nuclear index distribution was made uniform as an average index of the nucleus (Fig. 2(d)), the fit quality with Mie theory was greatly improved (Figs. 2(e)-(f))

#115619 - $15.00 USD Received 13 Aug 2009; revised 27 Sep 2009; accepted 28 Sep 2009; published 15 Oct 2009

whereas the fitted diameter became smaller, compare to the heterogeneous case, 7.41 and 9.05 μm, and even closer to the physical dimensions of the tomogram.

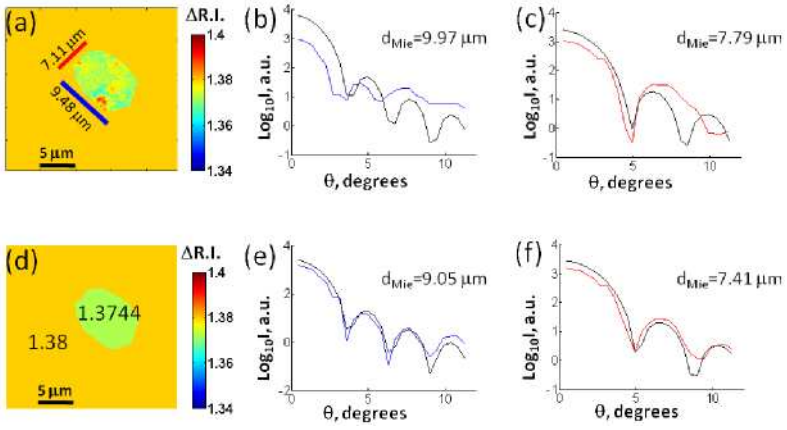

Fig. 2. Fitting the angular scattering distribution of nucleus with Mie theory: (a) The tomogram section of the nucleus is indicated with major axis (blue) and minor axis (red). (b) Angular scattering distribution along major axis (blue) and Mie theory fit (black). (c) Angular scattering distribution along major axis (red) and Mie theory fit (black). (d) Tomogram section of homogenized nuclear tomogram. (e) Scattering along major axis (blue) and Mie theory fit (black). (f) Scattering along minor axis (red) and Mie theory fit (black). The color bars in (a) and (d) indicate refractive index at the wavelength of 633 nm.

A similar procedure was repeated with the nucleolus scattering analysis. The average refractive index of the nucleolus of 1.384, taken from original index tomogram, was used in the calculation, and the average index of the nucleolus-less nucleus of 1.374 also taken from the original tomogram. The diameters extracted from Mie theory fitting were 2.8 and 5.3 μm, while the respective lengths from the tomogram were 2.9 and 5.2 μm.

The result of this single cell study is directly applicable to the modeling of scattering from multi-cellular samples. Under the condition that cells scatter independently, Mie theory should be applicable to extracting a distribution of the organelle diameters for the specific detection axis. This extraction is possible as long as the signal from the organelles of interest is well separated from the rest of the scattering and the type of the organelles' size distribution in the measurement volume is determined.

5. Relative strength of scattering from various organelles

Finally, we studied the relative strengths of the scattering from the different organelles. In order to determine the morphology of the specific organelles such as nuclei from the light scattering measurement of the entire cell, the measurement must be sufficiently sensitive to account for baseline scattering from the whole cell.

The knowledge of the relative strengths of light scattering among various intracellular compartments can serve as an important criterion in designing light scattering spectroscopy systems. For this purpose, we compared scattering from three major categories: whole cell, entire intracellular particles and nucleus. The original tomogram (Fig. 3(a)), the same tomogram with the index of the medium set to be the same as the average index of the cell (Fig. 3(b)), and the nuclear tomogram (Fig. 3(c)) were prepared for each of the three categories. Figure 3(a) represents a cell in suspension, while Fig. 3(b) simulates an intact cell in cell monolayer or tissues, in which scattering at the cell boundary is attenuated.

#115619 - $15.00 USD Received 13 Aug 2009; revised 27 Sep 2009; accepted 28 Sep 2009; published 15 Oct 2009

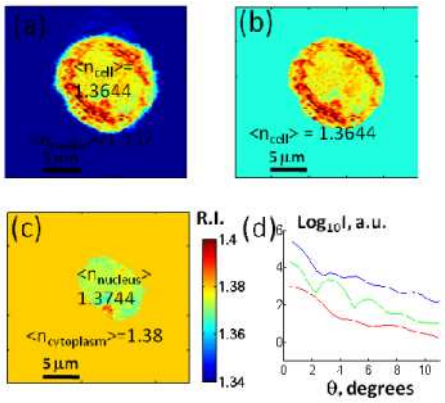

Fig. 3. Comparison of relative scattering strengths among the whole cell, the entire intracellular organelles, and the nucleus: (a) Tomogram of the HT29 cell in culture medium. (b) Tomogram of HT29 cell with index in the media matched to an average index of the whole cell. (c) Nuclear tomogram surrounded by the average index of the cytoplasm. Scale bars indicate 5 μm. (d) Angular scattering spectrum from the whole cell in the culture medium (blue), index-matched cell (green) and nucleus (red).

Angular scattering spectra were first calculated following Eq. (1) and then averaged azimuthally to sum up all the scattering signals (Fig. 3(d)). The angular scattering of the nucleus is about 2 orders of magnitude smaller than the scattering of the whole cell in the culture media. This agrees well with the expectation from the relative index contrast of the nucleus to the cytoplasm, about 0.996, and the relative index contrast of the cell to the medium of 1.021. Notably, the shape of the nuclear scattering spectrum (solid red in Fig. 3(d)) does not exhibit obvious oscillatory features associated with the cross-sectional diameters of the nucleus observed in Figs. 3(b)-(c), which is due to the azimuthal averaging of the spectrum, equivalent to the averaging of the various cross-sectional diameters.

When nuclear scattering is compared to the scattering of the index-matched cells, nuclear scattering is about an order of magnitude weaker, which means that the scattering from intracellular particles outweighs the scattering from the nucleus. The scattering of the nucleolus was about an order of magnitude weaker than the scattering of the nucleus (Fig. 1.e vs. Figure 1.f).

In conventional light scattering, the nuclear index was estimated between 1.39 and 1.46, providing on index contrast of 1.04 to 1.07 [1, 7, 10], which is relatively higher than our measurements. One possibility is that the nuclear index may depend on the type of cells and the conditions of cell culture such as population of cells. But index contrast was determined in conventional light scattering studies from the fitting of the scattering data with spherical model of nuclei or shell model of nucleus inside the cell. The assumption of the cell size distribution had to be made to take the statistical considerations on the cell shapes, which can degrade the accuracy of the fitting. On the other hand, the approach presented here is deterministic and model-independent such that our estimation on the relative strengths of intracellular organelles has superior accuracy to the conventional light scattering approach. Given the results of this single cell study, the models in which nuclei have significant contribution to the scattering may need to be re-evaluated. We note that previous studies based on the phase microscopy also provide further supporting evidence on weak index contrast of nucleus. From simultaneous detection of phase shift and cell height using phase microscopy and confocal microscopy, respectively, the index of nucleus was found to be almost the same as that of the cytoplasm [23]. Ross *et al.* and Barer *et al.* developed methods of measuring indices of cytoplasm and nucleus using phase contrast microscopy and interferometric microscopy, and reported that their indices are almost the same [24, 25]. Using the same method, Brunsting *et al.* measured the indices of cytoplasm and nucleus of

#115619 - $15.00 USD Received 13 Aug 2009; revised 27 Sep 2009; accepted 28 Sep 2009; published 15 Oct 2009

Chinese hamster ovary cells to be 1.3703 and 1.392, respectively [12], giving the relative refractive index contrast of 1.016.

6. Summary

In summary, we have demonstrated a method for determining scattering spectra of any sub-cellular organelles in the intact cells, given that the organelles have clearly defined borders. The validity of the spherical cell model for the non-spherical shape of organelles was confirmed in single cells. The nuclear contribution to the scattering was estimated based on the direct measurement of the refractive index inside single cells. The value of nuclear index and, consequently, scattering was lower than the one obtained with indirect modeling of the cell scattering, and raises the issue of the validity of the models. In the future work, we will extend the single cell results to the study of diagnostically relevant angles around exact backscattering with the use of the conventional light scattering spectroscopy.

Acknowledgments

This work was funded by the National Center for Research Resources of the National Institutes of Health (P41-RR02594-18), the National Science Foundation (DBI-0754339) and Hamamatsu Corporation.

#115619 - $15.00 USD Received 13 Aug 2009; revised 27 Sep 2009; accepted 28 Sep 2009; published 15 Oct 2009